npj | digital medicine

Article

Published in partnership with Seoul National University Bundang Hospital

https://doi.org/10.1038/s41746-025-02161-5

Deep learning-based brain age predicts stroke recurrence in acute ischemic cerebrovascular disease

Hongyu Zhou[1,2,8], Ziyang Liu[3,8], Jing Jing[1,2,4], Hongqiu Gu[1,2], Lingling Ding[1,2,5], Yingyu Jiang[1,2], Hao Liu[3], Jinxin Zhao[6], Wanlin Zhu[1,2,4], Yuesong Pan[1,2], Yong Jiang[1,2], Xia Meng[1,2], Xuewei Xie[1,2], Zhe Zhang[1,2,4], Jian Cheng[6], Yubo Fan[3], Yilong Wang[1,2], Xingquan Zhao[1,2,5], Hao Li[1,2], Zixiao Li[1,2,5] ✉, Tao Liu[3] ✉ & Yongjun Wang[1,2,5,7] ✉

Acute ischemic cerebrovascular disease (AICVD) exhibits high recurrence rates, necessitating novel biomarkers for refined risk stratification. While MRI-derived brain age correlates with stroke incidence, its prognostic utility for recurrence is unestablished. We developed the Mask-based Brain Age estimation Network (MBA Net), a deep learning framework designed for AICVD patients. MBA Net predicts contextual brain age (CBA) in non-infarcted regions by masking acute infarcts on T2-FLAIR images, thereby mitigating the confounding effects of dynamic infarcts during acute-phase neuroimaging. The model was trained on data from 5353 healthy individuals and then applied to a multicenter cohort of 10,890 AICVD patients. Brain age gap (BAG), defined as the deviation between CBA and chronological age, independently predicted stroke recurrence at both 3 months and 5 years, outperforming chronological age. Incorporating BAG into established prediction models significantly improved discriminative performance. These findings support brain age's potential utility in AI-driven precision strategies for secondary stroke prevention.

Acute ischemic cerebrovascular disease (AICVD) is distinguished by high recurrence rates, which impairs prognosis and imposes heavy burdens on individuals and society[1]. Despite the administration of genotype-guided antiplatelet therapy, a residual recurrence rate of approximately 6% persists[2]. The identification of novel biomarkers capable of refining recurrence risk stratification may facilitate more targeted therapeutic interventions and improve long-term prognosis[3].

Brain age, a comprehensive metric of brain health, is derived from neuroimaging data through artificial intelligence (AI) algorithms[4]. The deviation between brain age and chronological age, referred to as the brain age gap (BAG), is increasingly recognized as a sensitive marker for assessing brain aging related to various diseases, such as neurodegenerative disorders, stroke, and psychiatric diseases[5–8]. A BAG greater than 0 indicates that an individual's brain age exceeds their chronological age[9]. Several studies have highlighted a strong correlation between BAG and vascular risk factors, including hypertension, diabetes, and smoking[10–12]. Moreover, evidence suggests that an increased BAG is associated with an elevated risk of stroke[13]. However, the relationship between BAG and stroke recurrence remains unclear.

Given that stroke recurrence predominantly occurs during the acute phase and clinical guidelines recommend the early initiation of antiplatelet therapy in eligible patients, investigating the association between acute phase brain age prediction and recurrence risk is of clinical significance[14–17]. Previous research on brain age prediction in patients with ischemic cerebrovascular disease has primarily focused on estimating whole-brain age[8,18,19]. However, during the acute phase of ischemic stroke, magnetic resonance imaging (MRI) phenotypes, such as infarct core and ischemic penumbra, undergo rapid changes[20]. Variability in the time from symptom onset to imaging completion, along with differences in infarct core growth rates, contributes to the heterogeneity of whole-brain age prediction in the

[1]Department of Neurology, Beijing Tiantan Hospital, Capital Medical University, Beijing, China. [2]China National Clinical Research Center for Neurological Diseases, Beijing, China. [3]Beijing Advanced Innovation Center for Biomedical Engineering, School of Biological Science and Medical Engineering, Beihang University, Beijing, China. [4]Tiantan Neuroimaging Center of Excellence, Beijing Tiantan Hospital, Capital Medical University, Beijing, China. [5]Research Unit of Artificial Intelligence in Cerebrovascular Disease, Chinese Academy of Medical Sciences, Beijing, China. [6]School of Computer Science and Engineering, Beihang University, Beijing, China. [7]Advanced Innovation Center for Human Brain Protection, Capital Medical University, Beijing, China. [8]These authors contributed equally: Hongyu Zhou, Ziyang Liu. ✉e-mail: lizixiao2008@hotmail.com; tao.liu@buaa.edu.cn; yongjunwang@ncrcnd.org.cn

acute phase. Prioritizing the analysis of non-infarcted brain regions while minimizing the impact of acute infarcts may provide a promising strategy to enhance clinical applicability in patients with AICVD.

Hence, in the present study, we developed a Mask-based Brain Age estimation Network (MBA Net) to predict the non-infarcted brain age, termed the *Contextual Brain Age* (CBA). First, we trained and validated MBA Net using T2-fluid-attenuated inversion recovery (T2-FLAIR) imaging data from 5353 healthy individuals, with image masks generated through an automated computational algorithm (Fig. 1a). Subsequently, we applied MBA Net in a large, multicenter, prospective stroke cohort involving 10,890 patients with AICVD. For each patient, image masks were constructed based on infarct regions. The masked T2-FLAIR images were then processed through the MBA Net to estimate the CBA and calculate the BAG (Fig. 1b). Furthermore, we demonstrated that BAG serves as an independent predictor of both short-term and long-term stroke recurrence risk in patients with AICVD (Fig. 1c).

Results

Mask-based Brain Age estimation Network and contextual brain age

During the training phase of MBA Net, 5353 T2-FLAIR images from healthy individuals were employed, sourced from two publicly accessible datasets and one community cohort: the Open Access Series of Imaging Studies (OASIS), the Alzheimer's Disease Neuroimaging Initiative (ADNI), and the PolyvasculaR Evaluation of Cognitive Impairment and Stroke (PRECISE) (Supplementary Table 1)[21–23]. The healthy dataset was randomly divided into training (80%, $n = 4265$), validation (10%, $n = 544$), and test (10%, $n = 544$) subsets. The validation set was utilized for model

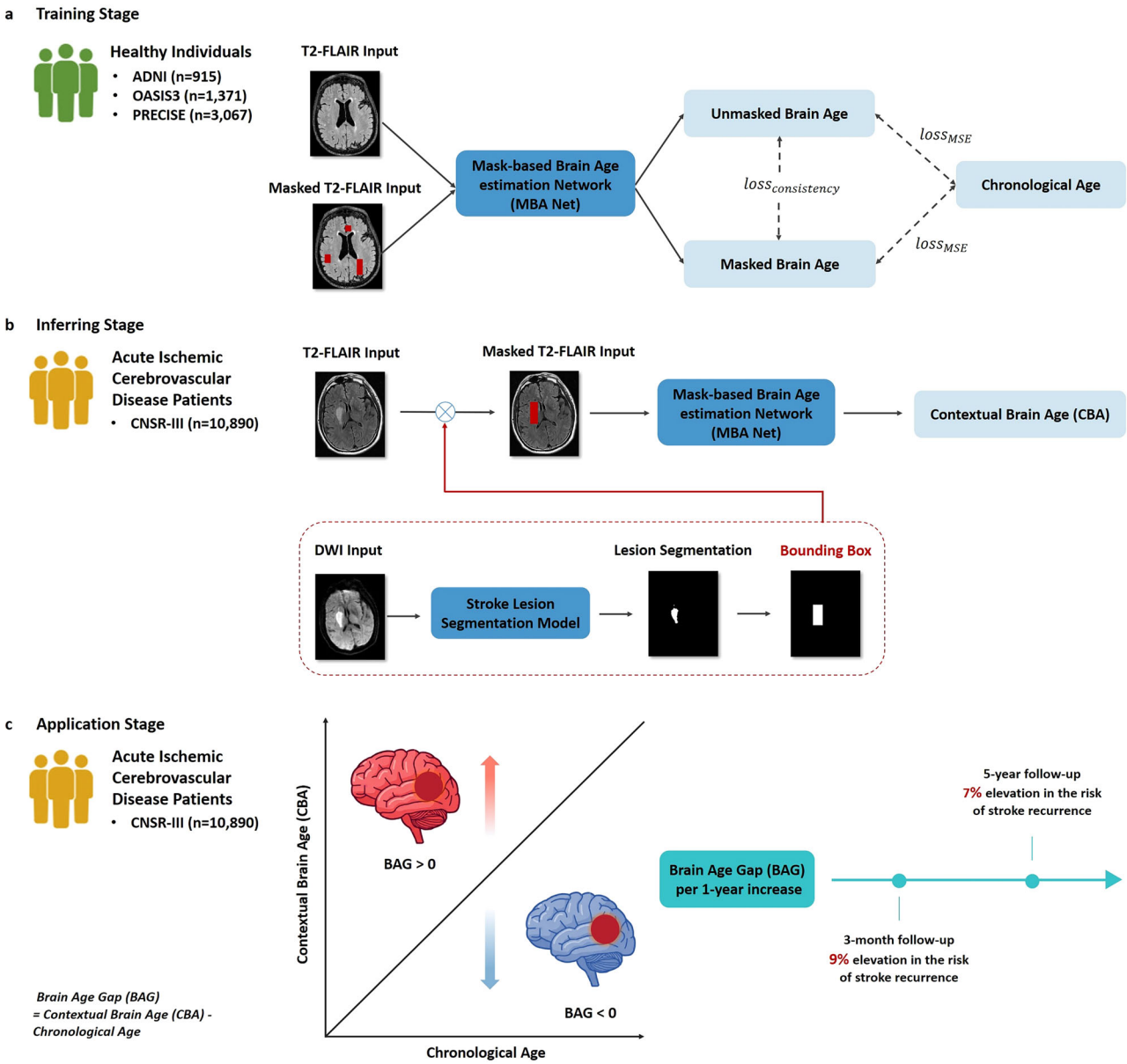

Fig. 1 | Overview of the study design. a Training procedure of the Mask-based Brain Age estimation Network (MBA Net). The model was developed to predict consistent brain age values for both masked and unmasked T2 fluid-attenuated inversion recovery (T2-FLAIR) images in heathy individuals. **b** Inference phase of contextual brain age (CBA) for patients with acute ischemic cerebrovascular disease (AICVD). The infarct lesion segmentation maps were converted into rectangular masks and subsequently applied to T2-FLAIR images to generate the corresponding masked T2-FLAIR images. These images were then processed through the MBA Net to estimate CBA and calculate the brain age gap (BAG). **c** Clinical application of the BAG in AICVD. For each additional year of BAG, the risks of stroke recurrence increased by 9% at 3 months and by 7% at 5 years.

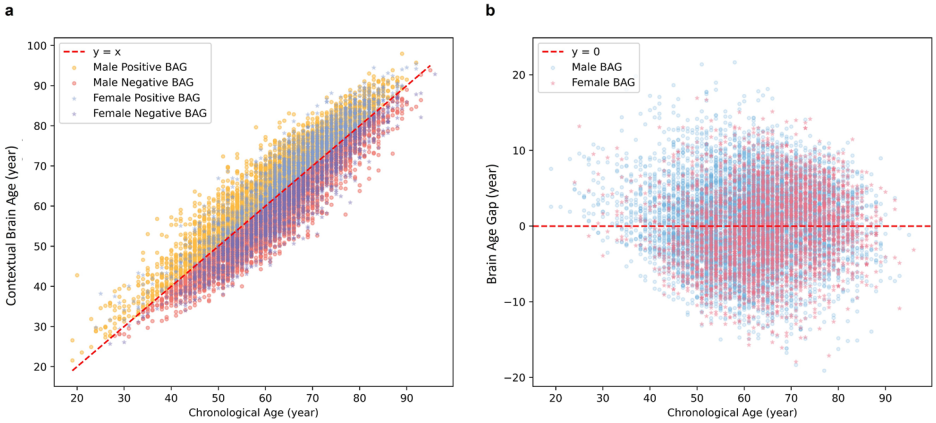

Fig. 2 | Scatterplots illustrating the relationships between contextual brain age (CBA), brain age gap (BAG), and chronologic age. a Scatterplots of CBA per chronological age. Yellow and orange circles indicate male patients with positive and negative BAG, respectively, while blue and purple pentagrams represent female patients with positive and negative BAG, respectively. **b** Scatterplots of BAG per chronological age. Blue circles represent male patients, and red pentagrams represent female patients.

Table 1 | Multivariable linear regression of the clinical phenotypes with brain age gap (BAG) in patients with acute ischemic cerebrovascular disease

Clinical phenotypes	BAG coefficient	95% CI		*p* Value
		Lower	Upper	
Male	0.13	0.41	0.90	<0.0001
History of ischemic stroke	1.94	1.69	2.18	<0.0001
History of hypertension	0.64	0.43	0.84	<0.0001
History of diabetes mellitus	0.48	0.25	0.72	<0.0001
History of hypercholesterolemia	0.01	−0.35	0.37	0.96
Previous or current smoking	0.14	−0.09	0.37	0.24
Pre-stroke mRS score 2-5	0.18	0.18	0.88	0.003

CI confidence interval, *mRS* modified Rankin Scale.

optimization, including performance monitoring (loss and mean absolute error [MAE]), hyperparameter tuning (i.e., learning rate and consistency regularization weight), and early stopping to prevent overfitting. To enhance the model's generalizability in acute ischemic cerebrovascular contexts, simulated lesion masks were applied to healthy T2-FLAIR images during training as a data augmentation technique. MBA Net demonstrated high predictive accuracy, achieving an MAE of 1.58 years ($R^2 = 0.92$) on the training set and 3.27 years ($R^2 = 0.89$) on the test set. Comparative evaluation against existing models showed the superior performance of MBA Net, as detailed in Supplementary Table 2. Among participants in the test set, a one-way analysis of variance revealed no significant differences in mean BAG values across cohorts. In contrast, analysis of covariance adjusting for age and sex indicated significant differences in BAG values ($F = 81.2$, $p < 0.0001$) and chronological age ($F = 390.7$, $p < 0.0001$), but not in sex distribution ($F = 3.4$, $p = 0.07$) (Supplementary Table 3).

In the inference process, the model estimated the CBA of 10,890 patients with AICVD from the Third China National Stroke Registry (CNSR-III) study (Supplementary Fig. 1, Supplementary Table 1)[24]. All included patients underwent high-quality T2-FLAIR and diffusion-weighted imaging (DWI) scans. Baseline characteristics of both included and excluded patients from the CNSR-III study are detailed in Supplementary Table 4. To enable lesion-aware inference, infarct regions were segmented from DWI scans using a pre-trained nnUNet model[25]. Corresponding lesion masks were represented by minimum bounding rectangles and applied to the respective T2-FLAIR images. These masked images were then input into MBA Net for CBA estimation. MBA Net exhibited robust performance in predicting CBA, as shown by MAE = 4.21 years, $R^2 = 0.91$. The mean CBA was 62.4 ± 12.4 years, while the mean BAG was 0.2 ± 5.3 years (Supplementary Table 1). Scatterplots illustrating the relationships among CBA, BAG, and chronological age are shown in Fig. 2. Notably, there was no significant correlation between BAG and chronological age ($r = 0.004$, $p = 0.65$).

To evaluate the effect of lesion masking on brain age estimation, BAG values derived from masked inputs (i.e., CBA) were compared with those from unmasked inputs (i.e., standard brain age) in patients with AICVD. The unmasked brain age was estimated using the ScaledDense model, which yielded an MAE of 4.0 years and an R^2 of 0.91[26]. The mean unmasked brain age was 62.2 ± 12.3 years, with a corresponding mean BAG of −0.1 ± 5.0 years. Of note, unmasked BAG was significantly associated with the interval from symptom onset to imaging ($r = 0.02$, $p = 0.01$), whereas masked BAG showed no such association ($r = -0.002$, $p = 0.86$). Besides, unmasked BAG demonstrated a negative correlation with infarct volume ($r = -0.41$, $p < 0.001$). Despite the application of lesion-masking techniques, masked BAG remained inversely correlated with infarct volume ($r = -0.38$, $p < 0.001$).

Risk factors associated with BAG in patients with AICVD

The analysis of BAG across various clinical phenotypes revealed significantly higher BAG levels in male patients, as well as in those with a history of ischemic stroke, hypertension, diabetes mellitus, hypercholesterolemia, smoking, or pre-stroke dependency (defined as a pre-stroke modified Rankin Scale [mRS] score of 2-5) (Supplementary Fig. 2). Furthermore, multivariable linear regression analysis, incorporating the aforementioned variables, identified significant associations between elevated BAG levels and male, medical history (ischemic stroke, hypertension, and diabetes mellitus), as well as pre-stroke dependency (Table 1).

Association between BAG and the risk of stroke recurrence

During the short-term 3-month follow-up period, 6.1% (664/10,890) of patients had a recurrent stroke, 6.6% (720/10,890) of patients had a composite vascular event, and 5.7% (623/10,890) of patients had a new ischemic stroke (Table 2). Over the subsequent long-term 5-year follow-up period, 15.7% (1707/10,890) of patients experienced recurrent stroke, 17.6% (1917/10,890) had new composite vascular events, and 14.4% (1565/10,890) encountered new ischemic stroke (Table 2).

Each additional year of BAG was associated with a 9% increase in the risk of stroke recurrence (adjusted hazard ratios [HR] = 1.09, 95% confidence interval [CI] = 1.07–1.11), an 8% increase in the risk of composite vascular events (adjusted HR = 1.08, 95% CI = 1.07–1.10), and a 9% increase in the risk of ischemic stroke (adjusted HR = 1.09, 95% CI = 1.07–1.11) within 3 months (Table 2). Over a 5-year follow-up, the corresponding HRs were 1.07 (95% CI = 1.06–1.08) for stroke recurrence, 1.06 (95% CI = 1.05–1.07) for composite vascular events, and 1.07 (95% CI = 1.06–1.08) for ischemic stroke (Table 2). Competing-risk analysis using the Fine-Gray model, which accounted for death as a competing event,

Table 2 | Association between each one-year increase in brain age gap (BAG) and the risk of recurrent stroke in patients with acute ischemic cerebrovascular disease

Outcomes	Total events (%)	Crude HR (95%CI)	Crude SHR (95%CI)	Adjusted HR (95%CI)[b]	Adjusted SHR (95%CI)[b]
3 months					
Stroke	664(6.1)	1.08(1.07–1.10)	1.08(1.07–1.10)	1.09(1.07–1.11)	1.09(1.07–1.11)
Composite vascular events[a]	720(6.6)	1.07(1.06–1.09)	1.07(1.06–1.09)	1.08(1.07–1.10)	1.08(1.07–1.10)
Ischemic stroke	623(5.7)	1.09(1.07–1.10)	1.09(1.07–1.10)	1.09(1.07–1.11)	1.09(1.07–1.11)
1 year					
Stroke	1043(9.6)	1.10(1.08–1.11)	1.10(1.08–1.11)	1.10(1.08–1.11)	1.10(1.08–1.11)
Composite vascular events[a]	1117(10.3)	1.09(1.08–1.10)	1.09(1.08–1.10)	1.09(1.08–1.10)	1.09(1.08–1.10)
Ischemic stroke	959(8.8)	1.09(1.08–1.11)	1.10(1.08–1.11)	1.10(1.08–1.11)	1.10(1.08–1.11)
2 years					
Stroke	1311(12.0)	1.08(1.07–1.09)	1.08(1.07–1.09)	1.08(1.07–1.09)	1.08(1.07–1.09)
Composite vascular events[a]	1455(13.4)	1.07(1.06–1.08)	1.07(1.06–1.08)	1.07(1.06–1.08)	1.07(1.06–1.08)
Ischemic stroke	1205(11.1)	1.08(1.07–1.09)	1.08(1.07–1.09)	1.08(1.07–1.09)	1.08(1.07–1.09)
3 years					
Stroke	1488(13.7)	1.08(1.07–1.09)	1.08(1.07–1.09)	1.07(1.06–1.08)	1.07(1.06–1.08)
Composite vascular events[a]	1665(15.3)	1.07(1.06–1.08)	1.07(1.06–1.08)	1.07(1.05–1.08)	1.06(1.05–1.07)
Ischemic stroke	1363(12.5)	1.07(1.06–1.09)	1.07(1.06–1.09)	1.07(1.06–1.08)	1.07(1.06–1.08)
4 years					
Stroke	1610(14.8)	1.07(1.06–1.08)	1.07(1.06–1.08)	1.07(1.06–1.08)	1.07(1.06–1.08)
Composite vascular events[a]	1803(16.6)	1.07(1.06–1.07)	1.06(1.06–1.07)	1.06(1.05–1.07)	1.06(1.05–1.07)
Ischemic stroke	1474(13.5)	1.07(1.06–1.08)	1.07(1.06–1.08)	1.07(1.06–1.08)	1.07(1.06–1.08)
5 years					
Stroke	1707(15.7)	1.07(1.06–1.08)	1.07(1.06–1.08)	1.07(1.06–1.08)	1.07(1.06–1.08)
Composite vascular events[a]	1917(17.6)	1.06(1.05–1.07)	1.06(1.05–1.07)	1.06(1.05–1.07)	1.06(1.05–1.07)
Ischemic stroke	1565(14.4)	1.07(1.06–1.08)	1.07(1.06–1.08)	1.07(1.05–1.08)	1.06(1.05–1.08)

BMI body mass index, *CI* confidence interval, *HR* hazard ratio, *mRS* modified Rankin Scale, *NIHSS* National Institutes of Health Stroke Scale, *SHR* subdistributed hazard ratio, *TIA* transient ischemic attack, *TOAST* Trial of Org 10172 in Acute Stroke Treatment.

[a]Composite vascular events were defined as a composite of stroke, TIA, myocardial infarction, and vascular death.

[b]Adjusted model: age, sex, medical history (ischemic stroke, hypertension, and diabetes mellitus), pre-stroke mRS score, index event, NIHSS score, TOAST classification, and infarct volume.

confirmed that BAG remained independently associated with increased risks of stroke recurrence, composite vascular events, and ischemic stroke at both 3 months and 5 years (Table 2).

In the sensitivity analysis, patients were stratified by BAG using two grouping strategies. The first approach divided patients into a positive BAG group (BAG > 0) and a negative BAG group (BAG ≤ 0). Of the 10,890 patients included, 52.0% (5658) had a positive BAG and 48.1% (5242) had a negative BAG (Supplementary Table 5). Patients with a positive BAG had a significantly higher 3-month and 5-year risk of stroke recurrence than those with a negative BAG (3 months: adjusted HR = 2.23, 95% CI = 1.88–2.64; 5 years: adjusted HR = 1.62, 95% CI = 1.47–1.79). Similarly, positive BAG was independently associated with increased risk of composite vascular events (3 months: adjusted HR = 2.03, 95% CI = 1.73–2.38; 5 years: adjusted HR = 1.53, 95% CI = 1.39–1.68) and ischemic stroke (3 months: adjusted HR = 2.34, 95% CI = 1.96–2.79; 5 years: adjusted HR = 1.60, 95% CI = 1.44–1.78) (Supplementary Table 6). These findings were further supported by consistent trends observed in the cumulative incidence curves (Fig. 3a, b, Supplementary Figs. 3a, b and 4a, b).

In a secondary stratification analysis, patients were categorized into three groups according to a BAG threshold of ±5 years, a cutoff selected to approximate the MAE of 4.21 years observed in the CNSR-III cohort: accelerated aging (BAG > 5), normal aging (−5 ≤ BAG ≤ 5), and decelerated aging (BAG < −5). Among 10,890 patients, 7142 (65.6%) were classified as normal aging, 1961 (18.0%) as accelerated aging, and 1787 (16.4%) as decelerated aging (Supplementary Table 7). Compared with the normal aging group, patients in the accelerated aging group had significantly increased risks of stroke recurrence (3 months: adjusted HR = 1.67, 95% CI = 1.40–1.98; 5 years: adjusted HR = 1.55, 95% CI = 1.38–1.73), composite vascular events (3 months: adjusted HR = 1.62, 95% CI = 1.37–1.92; 5 years: adjusted HR = 1.53, 95% CI = 1.37–1.70), and ischemic stroke (3 months: adjusted HR = 1.64, 95% CI = 1.37–1.97; 5 years: adjusted HR = 1.52, 95% CI = 1.35–1.70). In contrast, the decelerated aging group showed substantially reduced risks of stroke recurrence (3 months: adjusted HR = 0.41, 95% CI = 0.30–0.55; 5 years: adjusted HR = 0.54, 95% CI = 0.45–0.64), composite vascular events (3 months: adjusted HR = 0.51, 95% CI = 0.39–0.66; 5 years: adjusted HR = 0.64, 95% CI = 0.55–0.75), and ischemic stroke (3 months: adjusted HR = 0.42, 95% CI = 0.31–0.57; 5 years: adjusted HR = 0.54, 95% CI = 0.46–0.65) (Supplementary Table 8). Cumulative incidence curves were consistent with these associations (Fig. 3c, d, Supplementary Figs. 3c, d and 4c, d).

During the 3-month follow-up period, 51 patients experienced hemorrhagic stroke, with the cumulative number of events increasing to 170 at 5 years. In the binary BAG classification, no significant difference in the 3-month risk of hemorrhagic stroke was observed between the negative

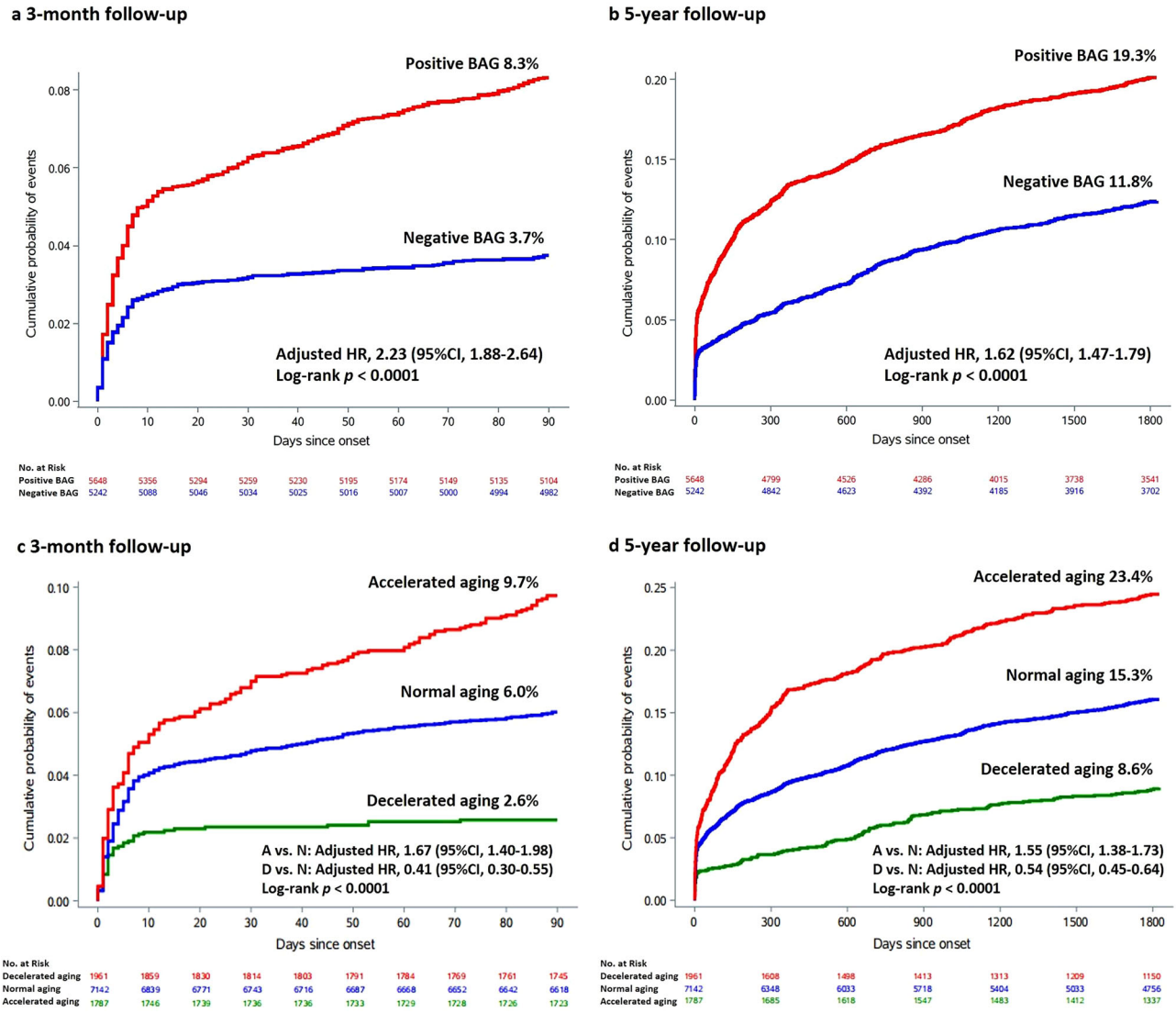

Fig. 3 | Cumulative probability of recurrent stroke stratified by brain age gap (BAG) at 3 months and 5 years. Time to outcome events were graphically presented using Kaplan–Meier curves and compared by the log-rank test. (**a**) and (**b**) show cumulative probability of recurrent stroke at 3 months and 5 years, respectively, based on binary BAG classification (positive BAG: red line; negative BAG: blue line). Adjusted covariates included age, sex, body mass index (BMI), medical history (ischemic stroke, coronary heart disease, hypertension, and diabetes mellitus), smoking history, pre-stroke modified Rankin Scale (mRS) score, National Institutes of Health Stroke Scale (NIHSS) score, index event, and Trial of Org 10172 in Acute Stroke Treatment (TOAST) classification. (**c**) and (**d**) present cumulative probability at 3 months and 5 years, respectively, based on three-level BAG classification (accelerated aging: red line; normal aging: blue line; decelerated aging: green line). The multivariable model adjusted for age, sex, BMI, medical history (ischemic stroke, hypertension, and diabetes mellitus), smoking history, pre-stroke mRS score, NIHSS score, index event, TOAST classification and infarct volume.

BAG and positive BAG groups (0.6% vs. 0.3%, $p = 0.07$). However, the negative BAG group had a significantly higher risk of hemorrhagic stroke compared to the positive BAG group at 5 years (2.1% vs. 1.0%, $p < 0.001$) (Supplementary Table 9). When stratified by three-level BAG classification, the risk of hemorrhagic stroke at both 3 months and 5 years was highest in the accelerated aging group and lowest in the decelerated aging group, with the normal aging group serving as reference (3 months: 0.8% vs. 0.5% vs. 0.1%, $p = 0.01$; 5 years: 2.5% vs. 1.5% vs. 0.7%, $p < 0.001$) (Supplementary Table 10).

Interaction between risk factors and BAG in relation to stroke recurrence

Interaction analyses were performed following stratification by age, sex, body mass index (BMI), medical history (ischemic stroke, coronary heart disease, hypertension, and diabetes mellitus), smoking status, diagnosis, pre-stroke mRS score, and Trial of Org 10172 in Acute Stroke Treatment (TOAST) classification. Each one-year increase in the BAG was associated with a higher risk of stroke recurrence at 3 months, except among patients with other determined etiology. A significant interaction between BAG and smoking status was observed for the 3-month recurrent stroke risk (Supplementary Table 11). Furthermore, BAG remained independently associated with an increased risk of stroke recurrence at 5 years, with the exception of patients diagnosed with transient ischemic attack (TIA) or those with other determined etiology. Interactions were significant between BAG and chronological age, history of diabetes mellitus, and pre-stroke mRS score in relation to 5-year stroke recurrence risk (Supplementary Table 12).

Predictive performance of BAG for stroke recurrence

The predictive performance of BAG was evaluated in comparison with chronological age for both short-term and long-term stroke recurrence. BAG demonstrated superior discriminative ability relative to chronological

Table 3 | Prediction performance of brain age gap (BAG) and chronological age on the risk of stroke recurrence in patients with acute ischemic cerebrovascular disease

Outcomes	C statistic (95% CI)[b]	*P* value	Brier score
3 months			
Stroke			
Chronological age	0.60 (0.58,0.63)	Ref.	0.05
BAG	0.65 (0.63,0.68)	<0.0001	0.05
Composite vascular events[a]			
Chronological age	0.60 (0.57,0.62)	Ref.	0.05
BAG	0.65 (0.63,0.67)	<0.0001	0.05
Ischemic stroke			
Chronological age	0.60 (0.57,0.62)	Ref.	0.04
BAG	0.65 (0.63,0.68)	<0.0001	0.04
1 year			
Stroke			
Chronological age	0.60 (0.58,0.62)	Ref.	0.07
BAG	0.67 (0.65,0.69)	<0.0001	0.07
Composite vascular events[a]			
Chronological age	0.60 (0.58,0.62)	Ref.	0.07
BAG	0.67 (0.65,0.69)	<0.0001	0.07
Ischemic stroke			
Chronological age	0.60 (0.58,0.62)	Ref.	0.07
BAG	0.67 (0.65,0.69)	<0.0001	0.07
2 years			
Stroke			
Chronological age	0.61 (0.59,0.63)	Ref.	0.08
BAG	0.67 (0.65,0.69)	<0.0001	0.08
Composite vascular events[a]			
Chronological age	0.60 (0.58,0.62)	Ref.	0.09
BAG	0.66 (0.64,0.68)	<0.0001	0.09
Ischemic stroke			
Chronological age	0.61 (0.59,0.63)	Ref.	0.08
BAG	0.67 (0.65,0.69)	<0.0001	0.08
3 years			
Stroke			
Chronological age	0.61 (0.59,0.63)	Ref.	0.09
BAG	0.67 (0.65,0.68)	<0.0001	0.09
Composite vascular events[a]			
Chronological age	0.61 (0.59,0.62)	Ref.	0.10
BAG	0.66 (0.64,0.67)	<0.0001	0.10
Ischemic stroke			
Chronological age	0.61 (0.59,0.63)	Ref.	0.08
BAG	0.67 (0.65,0.68)	<0.0001	0.08
4 years			
Stroke			
Chronological age	0.61 (0.60,0.63)	Ref.	0.10
BAG	0.66 (0.65,0.68)	<0.0001	0.10
Composite vascular events[a]			
Chronological age	0.61 (0.59,0.62)	Ref.	0.11
BAG	0.65 (0.64,0.67)	<0.0001	0.11
Ischemic stroke			
Chronological age	0.61 (0.60,0.63)	Ref.	0.09
BAG	0.66 (0.64,0.68)	<0.0001	0.09
5 years			
Stroke			
Chronological age	0.62 (0.60,0.64)	Ref.	0.10
BAG	0.66 (0.64,0.68)	<0.0001	0.10
Composite vascular events[a]			
Chronological age	0.61 (0.60,0.63)	Ref.	0.11
BAG	0.65 (0.63,0.66)	<0.0001	0.11
Ischemic stroke			
Chronological age	0.62 (0.60,0.64)	Ref.	0.10
BAG	0.66 (0.64,0.67)	0.0004	0.10

BMI body mass index, *CI* confidence interval, *mRS* modified Rankin Scale, *NIHSS* National Institutes of Health Stroke Scale, *TIA* transient ischemic attack, *TOAST* Trial of Org 10172 in Acute Stroke Treatment.

[a]Composite vascular events were defined as a composite of stroke, TIA, myocardial infarction, and vascular death.

[b]Adjusted model: age, sex, medical history (ischemic stroke, hypertension, and diabetes mellitus), pre-stroke mRS score, index event, NIHSS score, TOAST classification, and infarct volume.

age at 3 months (C-statistic: 0.65 vs. 0.60, $p < 0.0001$) and 5 years (C-statistic: 0.66 vs. 0.62, $p < 0.0001$) (Table 3). Similar findings were observed for the prediction of composite vascular events and recurrent ischemic stroke (Table 3). Brier scores were comparable between BAG and chronological age (Table 3).

To evaluate the incremental predictive value of BAG, we incorporated it into established clinical prediction models: the Stroke Prognosis Instrument (SPI-I), Stroke Prognosis Instrument II (SPI-II), Essen Stroke Risk Score (ESRS), and RRE-90 scores for patients with acute ischemic stroke (AIS), and the ABCD² score (age, blood pressure, clinical weakness, duration, and diabetes) for those with TIA[27–31]. Among patients with AIS, the addition of BAG significantly improved risk stratification for stroke recurrence at both 3 months and 5 years across all four models: SPI-I (3 months: ΔC statistic = 0.08, net reclassification improvement [NRI] =0.23, integrated discrimination improvement [IDI] = 0.01; 5 years: ΔC statistic = 0.06, NRI = 0.24, IDI = 0.02), SPI-II (3 months: ΔC statistic = 0.07, NRI = 0.23, IDI = 0.01; 5 years: ΔC statistic = 0.05, NRI = 0.23, IDI = 0.02), ESRS (3 months: ΔC statistic = 0.10, NRI = 0.24, IDI = 0.01; 5 years: ΔC statistic = 0.06, NRI = 0.25, IDI = 0.02), and RRE-90 scores (3 months: ΔC statistic = 0.08, NRI = 0.22, IDI = 0.01; 5 years: ΔC statistic = 0.07, NRI = 0.27, IDI = 0.02) (Table 4). Conversely, the incorporation of BAG into the ABCD² score yielded only modest improvements for patients with TIA (Table 4).

To further evaluate the independent contribution of BAG, it was integrated into multivariable Cox proportional hazards models that included conventional vascular risk factors, demographic characteristics, and relevant clinical features. BAG significantly enhanced prediction of stroke recurrence at 3 months and 5 years beyond the conventional clinical model alone (3 months: ΔC statistic = 0.06, NRI = 0.21, IDI = 0.01; 5 years: ΔC statistic = 0.03, NRI = 0.22, IDI = 0.02) (Table 5).

Discussion

In this study, we proposed a novel brain age prediction model, MBA Net, specifically designed for patients with AICVD. This model enabled the assessment of non-infarcted brain regions, thereby mitigating the influence of acute ischemic infarction. The results demonstrate that BAG is an independent predictor of both short-term and long-term risk of stroke recurrence in patients with AICVD, with superior predictive performance

Table 4 | Performance of established clinical prediction models combined with brain age gap (BAG) for predicting stroke recurrence

Outcomes	Patients with acute ischemic stroke								Patients with transient ischemic attack	
	SPI-I		SPI-II		ESRS		RRE-90		ABCD^2	
	Raw model	Raw model + BAG	Raw model	Raw model + BAG	Raw model	Raw model + BAG	Raw model	Raw model + BAG	Raw model	Raw model + BAG
3 months										
C statistic (95% CI)	0.55(0.53–0.57)	0.63(0.60–0.65)	0.55(0.53–0.57)	0.63(0.60–0.65)	0.52(0.51–0.54)	0.62(0.60–0.64)	0.56(0.54–0.58)	0.64(0.62–0.66)	0.58(0.50–0.66)	0.64(0.56–0.72)
ΔC statistic (95% CI)	Ref.	0.08(0.06–0.10)	Ref.	0.07(0.05–0.10)	Ref.	0.10(0.07–0.12)	Ref.	0.08(0.06–0.10)	Ref.	0.08(−0.07–0.18)
NRI (95% CI)	Ref.	0.23(0.16–0.30)	Ref.	0.23(0.16–0.30)	Ref.	0.24(0.16–0.31)	Ref.	0.22(0.16–0.31)	Ref.	0.09(−0.07–0.37)
IDI (95% CI)	Ref.	0.01(0.01–0.02)	Ref.	0.01(0.01–0.02)	Ref.	0.01(0.01–0.02)	Ref.	0.01(0.01–0.02)	Ref.	0.01(0.00–0.02)
Brier score	0.05	0.05	0.05	0.05	0.05	0.05	0.05	0.05	0.03	0.03
1 year										
C statistic (95% CI)	0.54(0.53–0.56)	0.64(0.62–0.65)	0.56(0.54–0.58)	0.64(0.62–0.66)	0.53(0.52–0.55)	0.64(0.62–0.65)	0.55(0.54–0.57)	0.65(0.63–0.66)	0.58(0.52–0.64)	0.65(0.59–0.70)
ΔC statistic (95% CI)	Ref.	0.10(0.08–0.12)	Ref.	0.08(0.07–0.09)	Ref.	0.10(0.08–0.12)	Ref.	0.09(0.07–0.11)	Ref.	0.06(−0.01–0.14)
NRI (95% CI)	Ref.	0.34(0.27–0.40)	Ref.	0.35(0.27–0.39)	Ref.	0.34(0.29–0.42)	Ref.	0.36(0.30–0.42)	Ref.	0.17(0.01–0.42)
IDI (95% CI)	Ref.	0.03(0.02–0.03)	Ref.	0.02(0.02–0.03)	Ref.	0.02(0.02–0.03)	Ref.	0.03(0.02–0.03)	Ref.	0.01(0.001–0.03)
Brier score	0.07	0.07	0.07	0.07	0.07	0.07	0.07	0.07	0.06	0.06
2 years										
C statistic (95% CI)	0.55(0.53–0.56)	0.62(0.61–0.64)	0.56(0.55–0.58)	0.63(0.61–0.64)	0.54(0.53–0.55)	0.62(0.60–0.63)	0.55(0.54–0.56)	0.63(0.61–0.64)	0.59(0.54–0.65)	0.64(0.59–0.70)
ΔC statistic (95% CI)	Ref.	0.07(0.06–0.09)	Ref.	0.06(0.05–0.07)	Ref.	0.08(0.06–0.09)	Ref.	0.08(0.06–0.09)	Ref.	0.04(0.01–0.07)
NRI (95% CI)	Ref.	0.28(0.23–0.35)	Ref.	0.28(0.22–0.33)	Ref.	0.28(0.23–0.35)	Ref.	0.30(0.25–0.35)	Ref.	0.09(−0.06–0.40)
IDI (95% CI)	Ref.	0.02(0.02–0.03)	Ref.	0.02(0.01–0.03)	Ref.	0.02(0.02–0.03)	Ref.	0.02(0.02–0.03)	Ref.	0.01(−0.001–0.02)
Brier score	0.08	0.08	0.08	0.08	0.08	0.08	0.08	0.08	0.06	0.06
3 years										
C statistic (95% CI)	0.55(0.53–0.56)	0.62(0.60–0.63)	0.57(0.56–0.58)	0.62(0.61–0.64)	0.54(0.53–0.56)	0.61(0.60–0.63)	0.55(0.54–0.56)	0.62(0.61–0.63)	0.58(0.52–0.63)	0.62(0.57–0.67)
ΔC statistic (95% CI)	Ref.	0.06(0.05–0.08)	Ref.	0.05(0.04–0.07)	Ref.	0.07(0.06–0.08)	Ref.	0.07(0.06–0.08)	Ref.	0.04(0.003–0.08)
NRI (95% CI)	Ref.	0.26(0.20–0.33)	Ref.	0.25(0.19–0.32)	Ref.	0.26(0.20–0.31)	Ref.	0.28(0.23–0.35)	Ref.	0.09(−0.06–0.37)
IDI (95% CI)	Ref.	0.02(0.02–0.03)	Ref.	0.02(0.02–0.03)	Ref.	0.02(0.02–0.03)	Ref.	0.02(0.02–0.03)	Ref.	0.01(0.00–0.02)
Brier score	0.09	0.09	0.09	0.09	0.09	0.09	0.09	0.09	0.07	0.07
4 years										
C statistic (95% CI)	0.55(0.54–0.56)	0.61(0.60–0.63)	0.57(0.55–0.58)	0.62(0.61–0.63)	0.54(0.53–0.56)	0.61(0.60–0.63)	0.55(0.54–0.56)	0.62(0.60–0.63)	0.57(0.52–0.62)	0.61(0.56–0.66)
ΔC statistic (95% CI)	Ref.	0.06(0.05–0.08)	Ref.	0.05(0.04–0.06)	Ref.	0.07(0.05–0.08)	Ref.	0.07(0.05–0.08)	Ref.	0.03(0.004–0.07)
NRI (95% CI)	Ref.	0.25(0.19–0.31)	Ref.	0.24(0.19–0.29)	Ref.	0.26(0.20–0.32)	Ref.	0.27(0.24–0.33)	Ref.	0.09(−0.03–0.40)
IDI (95% CI)	Ref.	0.02(0.02–0.03)	Ref.	0.02(0.02–0.03)	Ref.	0.02(0.02–0.03)	Ref.	0.02(0.02–0.03)	Ref.	0.01(0.00–0.02)
Brier score	0.10	0.10	0.10	0.10	0.10	0.10	0.10	0.10	0.07	0.07

Table 4 (continued) | Performance of established clinical prediction models combined with brain age gap (BAG) for predicting stroke recurrence

Outcomes	Patients with acute ischemic stroke								Patients with transient ischemic attack	
	SPI-I		SPI-II		ESRS		RRE-90		ABCD^2	
	Raw model	Raw model + BAG	Raw model	Raw model + BAG	Raw model	Raw model + BAG	Raw model	Raw model + BAG	Raw model	Raw model + BAG
5 years										
C statistic (95% CI)	0.55(0.54–0.57)	0.61(0.60–0.63)	0.57(0.56–0.58)	0.62(0.61–0.63)	0.54(0.53–0.55)	0.61(0.60–0.62)	0.55(0.54–0.56)	0.62(0.60–0.63)	0.57(0.52–0.62)	0.61(0.56–0.66)
ΔC statistic (95% CI)	Ref.	0.06(0.04–0.07)	Ref.	0.05(0.04–0.06)	Ref.	0.06(0.05–0.08)	Ref.	0.07(0.05–0.08)	Ref.	0.03(−0.005–0.07)
NRI (95% CI)	Ref.	0.24(0.19–0.29)	Ref.	0.23(0.18–0.29)	Ref.	0.25(0.20–0.31)	Ref.	0.27(0.22–0.30)	Ref.	0.08(−0.02–0.32)
IDI (95% CI)	Ref.	0.02(0.02–0.03)	Ref.	0.02(0.01–0.02)	Ref.	0.02(0.01–0.03)	Ref.	0.02(0.02–0.03)	Ref.	0.004(−0.001–0.02)
Brier score	0.11	0.11	0.11	0.11	0.11	0.11	0.11	0.11	0.09	0.09

ESRS Essen Stroke Risk Score, *IDI* integrated discrimination improvement, *NRI* net reclassification improvement, *SPI-I* Stroke Prognosis Instrument, *SPI-II* Stroke Prognosis Instrument II.

Table 5 | Incremental predictive value of brain age gap (BAG) for stroke recurrence beyond conventional clinical models

Outcomes	Conventional clinical model[a]	Conventional clinical model + BAG
3 months		
C statistic (95% CI)	0.59(0.56–0.61)	0.65(0.63–0.67)
ΔC statistic (95% CI)	Ref.	0.06(0.03–0.08)
NRI (95% CI)	Ref.	0.21(0.16–0.30)
IDI (95% CI)	Ref.	0.01(0.01–0.02)
Brier score	0.05	0.05
1 year		
C statistic (95% CI)	0.59(0.57–0.61)	0.65(0.64–0.67)
ΔC statistic (95% CI)	Ref.	0.06(0.04–0.08)
NRI (95% CI)	Ref.	0.30(0.24–0.37)
IDI (95% CI)	Ref.	0.02(0.02–0.03)
Brier score	0.07	0.07
2 years		
C statistic (95% CI)	0.60(0.58–0.61)	0.64(0.63–0.66)
ΔC statistic (95% CI)	Ref.	0.04(0.03–0.06)
NRI (95% CI)	Ref.	0.24(0.20–0.31)
IDI (95% CI)	Ref.	0.02(0.01–0.03)
Brier score	0.08	0.08
3 years		
C statistic (95% CI)	0.60(0.59–0.61)	0.64(0.62–0.65)
ΔC statistic (95% CI)	Ref.	0.04(0.03–0.05)
NRI (95% CI)	Ref.	0.23(0.19–0.28)
IDI (95% CI)	Ref.	0.02(0.01–0.02)
Brier score	0.09	0.09
4 years		
C statistic (95% CI)	0.60(0.58–0.61)	0.64(0.62–0.65)
ΔC statistic (95% CI)	Ref.	0.03(0.02–0.05)
NRI (95% CI)	Ref.	0.23(0.17–0.27)
IDI (95% CI)	Ref.	0.02(0.01–0.02)
Brier score	0.10	0.10
5 years		
C statistic (95% CI)	0.60(0.59–0.61)	0.63(0.62–0.65)
ΔC statistic (95% CI)	Ref.	0.03(0.02–0.04)
NRI (95% CI)	Ref.	0.22(0.16–0.26)
IDI (95% CI)	Ref.	0.02(0.01–0.02)
Brier score	0.11	0.11

IDI integrated discrimination improvement, *NRI* net reclassification improvement.
[a]Conventional clinical model included age, sex, body mass index, history of ischemic stroke, transient ischemic attack, coronary heart disease, hypertension, diabetes mellitus, hypercholesterolemia, smoking status, index event, National Institutes of Health Stroke Scale score on admission, pre-stroke modified Rankin Scale score, and Trial of Org 10172 in Acute Stroke Treatment classification.

compared to chronological age. Furthermore, the incorporation of BAG into established risk scores and conventional clinical models improved their discriminative ability. These findings underscore the potential of BAG to enhance individualized risk stratification and provide a clinically applicable tool to support AI-driven precision strategies in secondary stroke prevention.

T2-FLAIR imaging was selected as the primary MRI sequence for input into the MBA Net based on its clinical relevance, demonstrated predictive value, and practical implementation advantages. First, T2-FLAIR is routinely used in clinical practice to assess cerebrovascular disease burden, providing high sensitivity for chronic ischemic changes such as white matter hyperintensities (WMHs) and lacunar infarcts[32]. Second, prior studies have shown that T2-FLAIR features, particularly WMHs and vascular hyperintensities, are independently associated with an increased risk of stroke recurrence[33,34]. Third, T2-FLAIR is widely included in standard acute stroke MRI protocols and can be acquired without extending scan time or requiring additional sequences, supporting its broad applicability in real-world clinical settings[35].

In contrast to earlier methods that primarily relied on WMHs for brain age estimation, MBA Net employs a convolutional neural network (CNN) to extract features from the entire T2-FLAIR image[36,37]. A key innovation of the MBA Net is its robust lesion-masking mechanism, which suppresses signals from acute ischemic lesions, allowing the network to focus on more stable parenchymal features. This selective processing enhances the signal-to-noise ratio and improves the generalizability of learned representations. Owing to its comprehensive feature extraction capabilities and modular architecture, the MBA Net facilitates the identification of a wide range of structural brain abnormalities, including WMHs, chronic infarcts, and subtle parenchymal changes. Its compatibility with various CNN-based frameworks supports scalable implementation across clinical and research environments. Additionally, a consistency loss function specifically adapted to the MBA Net architecture was employed to minimize the discrepancy between predicted and chronological brain age, enhancing robustness across heterogeneous imaging inputs.

Our findings demonstrate a significant association between unmasked BAG and the time from symptom onset to imaging. In contrast, masked BAG exhibited no such association. This result is consistent with our foundational rationale for employing a lesion-masking approach to mitigate the confounding influence of acute infarcts on brain age estimation. Furthermore, comparative analyses revealed that masked BAG outperformed unmasked BAG in predicting stroke recurrence, thereby underscoring the enhanced clinical utility of the masking strategy in improving model robustness and predictive accuracy (Supplementary Tables 13, 14 and 15).

Despite the application of DWI-based masking to reduce the influence of acute infarcts on T2-FLAIR–derived brain age estimations, BAG remained inversely associated with infarct volume. This relationship likely reflects the distinct temporal dynamics and underlying pathophysiologic mechanisms of DWI and T2-FLAIR imaging in acute ischemic stroke[38]. DWI is highly sensitive to cytotoxic edema and can rapidly identify the infarct core within minutes of symptom onset, making it the preferred modality for delineating hyperacute ischemic injury[39]. In contrast, T2-FLAIR reflects vasogenic edema, which appears later and typically covers a broader ischemic region[38]. Although DWI and T2-FLAIR are recognized as complementary, the sensitivity of FLAIR to chronic ischemic changes may complicate the differentiation between new and old infarcts, especially when they coexist[32]. Therefore, DWI-based segmentation was utilized to define acute infarct regions, which subsequently generated corresponding lesion masks for the T2-FLAIR images. The observed inverse association between BAG and infarct volume may be attributable to the relatively delayed timing of MRI acquisition in the CNSR-III cohort (median, 2 days; interquartile range [IQR], 1–4 days). During this period, T2-FLAIR abnormalities can extend beyond the DWI-defined infarct core, potentially reflecting penumbral tissue[38]. Notably, even after adjustment for infarct volume, BAG remained independently associated with stroke recurrence, underscoring its predictive value beyond acute lesion burden. This further highlights the importance of early DWI application for infarct segmentation and mask generation in T2-FLAIR–based brain age modeling to improve prediction accuracy. Prior studies have shown that a mismatch pattern of positive DWI and negative T2-FLAIR can help identify patients with unknown stroke onset who may still benefit from thrombolytic therapy[35]. Future research is needed to assess the robustness and generalizability of the MBA Net model during the hyperacute phase of stroke, particularly in populations undergoing reperfusion therapy or early antiplatelet treatment, to firmly establish its broader clinical utility.

In the present study, BAG was evaluated as a continuous, binary, and three-category variable to assess its association with stroke recurrence risk. Across all analytic approaches, elevated BAG was consistently associated with an increased risk of both short-term and long-term stroke recurrence in patients with AICVD. Crucially, in the three-category analysis, patients classified in the accelerated aging group demonstrated significantly higher risks of both ischemic and hemorrhagic stroke compared with those in the normal aging group. Given that antiplatelet therapy is a cornerstone of acute ischemic stroke management and requires careful risk-benefit assessment, these findings suggest that BAG may serve as a useful biomarker to inform individualized therapeutic decisions[40]. Future efforts could focus on developing BAG-centered, AI-driven tools to identify patients most likely to benefit from antiplatelet therapy, thereby improving secondary prevention while minimizing treatment-related harms.

Subgroup analyses revealed no significant association between accelerated brain aging and stroke recurrence among patients with other determined etiology. This finding aligns with the underlying pathophysiology, as these etiologies are often driven by systemic conditions (e.g., coagulopathies) rather than primary cerebrovascular pathology[41]. Similarly, in patients with TIA, an elevated BAG was not significantly associated with 5-year stroke recurrence, and its incremental predictive value in TIA risk models was limited. This likely reflects the generally milder clinical course and lower burden of brain aging-related risk factors in patients with TIA, thereby constraining the predictive utility of BAG[42]. Collectively, these findings suggest that BAG may serve as a valuable biomarker for developing novel stroke classification systems that integrate aging-related mechanisms with recurrence risk, offering evidence to support precision interventions based on brain aging.

We observed no significant correlation between BAG and chronological age, suggesting our model effectively minimized age-related confounding. Importantly, BAG outperformed chronological age in predicting stroke recurrence risk. Several factors may account for this finding. First, our results align with previous studies indicating that accelerated brain aging is closely associated with a range of vascular risk factors, underscoring the clinical relevance of BAG in stratifying stroke recurrence risk[13,43]. Second, aging is an asynchronous process across organ systems[44]. As a composite indicator of brain health, BAG may capture multidimensional features of brain aging more effectively than chronological age, thus offering greater specificity in identifying individuals at higher stroke recurrence risk[45,46]. Third, BAG was estimated during the acute stroke phase using a masking technique to exclude acute infarcts, aiming to approximate the pre-stroke brain state. This method provides a reasonable proxy given limited pre-stroke imaging availability. Furthermore, as the risk of stroke recurrence is highest in the acute phase, BAG derived from non-infarcted regions may reflect both underlying brain aging and latent imaging features relevant to recurrence risk[14]. Notably, we also identified substantial variation in BAG values among patients with multiple vascular risk factors (Fig. 4). This suggests potential individual resilience or tolerance mechanisms to brain aging in response to cerebrovascular stress, a finding consistent with prior research indicating that the aging process is regulated by a confluence of genetic, environmental, and other factors[9]. Future studies should incorporate multi-omics approaches, including genomics, epigenomics, and metabolomics, to deepen the understanding of the relationship between brain aging and stroke recurrence risk[47,48].

In this study, the inclusion of BAG in established risk scores and conventional clinical models was associated with a significant improvement

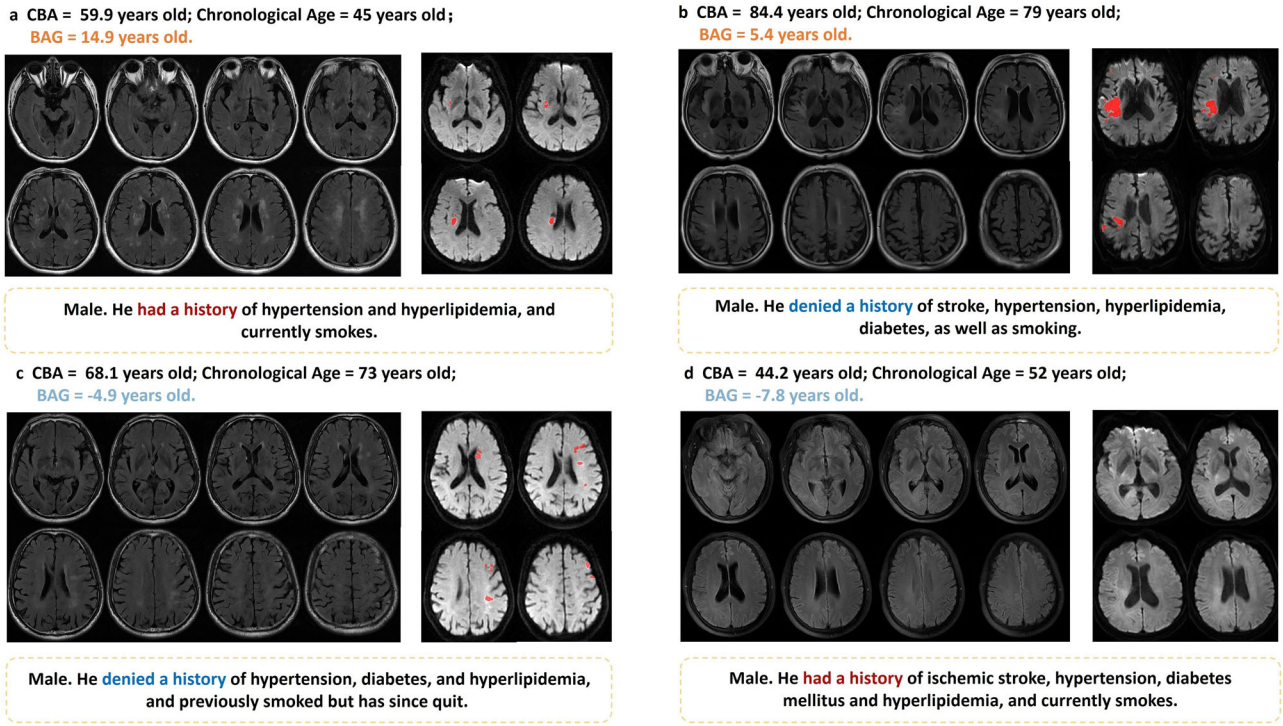

Fig. 4 | Examples of mismatch between brain age gap (BAG) and vascular risk factors. a The patient's contextual brain age (CBA) was "older" than chronological age. He had multiple vascular risk factors. **b** The patient's CBA was "older" than chronological age. He did not have multiple vascular risk factors. **c** The patient's CBA was "younger" than chronological age. He did not have multiple vascular risk factors. **d** The patient's CBA was "younger" than chronological age. He had multiple vascular risk factors. The image on the left depicts an axial T2-fluid-attenuated inversion recovery scan, while the image on the right displays a diffusion-weighted imaging scan, with the red marker highlighting the infarct lesion.

in the prediction of stroke recurrence, suggesting that BAG may capture neurobiological features not fully reflected by traditional clinical variables. This additional discriminative value may facilitate more precise risk stratification and support the development of personalized strategies for secondary stroke prevention. Beyond these immediate findings, the translational potential of BAG extends to several promising avenues. The integration of BAG with other aging-related biomarkers, such as telomere length and epigenetic age, may enable the construction of more comprehensive multi-omics models of brain aging and provide further insights into the complex interplay between brain aging and cerebrovascular disease[49,50]. Leveraging insights from psychiatric disease research, BAG also holds promise as an informative imaging endpoint in cerebrovascular disease clinical trials, potentially offering novel evaluative frameworks for early intervention and contributing to the elucidation of underlying pathophysiological mechanisms[51,52]. Furthermore, the successful establishment of brain age prediction models in macaques and rats lays a crucial foundation for closely linking preclinical studies with clinical practice[53,54]. Exploring therapeutic strategies to effectively mitigate the recurrence risk associated with accelerated brain aging has the potential to pave groundbreaking pathways for improving stroke outcomes.

Some limitations need to be considered. First, despite the application of statistical bias correction methods, residual uncertainty or systematic bias in brain age prediction may persist, potentially resulting from heterogeneity in age distributions among cohorts within the training dataset and between the training and inference datasets. To enhance model generalizability and clinical utility, future research may consider optimizing the age composition of training cohorts based on specific analytical objectives. This could involve ensuring a more uniform distribution of age groups within the training data or selecting datasets with age structures that closely match those of the intended target population[55]. Such strategies are expected to improve the model's performance and applicability in diverse clinical contexts. Second, the absence of a comprehensive Explainable AI (XAI) evaluation limits the interpretability of the MBA Net model. Further investigations should incorporate XAI techniques to more deeply explore the biological significance of brain age models in cerebrovascular disease from a radiomics perspective[56]. Third, the clinical application analysis was based solely on a cohort of Chinese patients. Given that stroke is influenced by various factors, including genetics, ethnicity, and lifestyle, additional validation in diverse, multi-ethnic populations is necessary to confirm the broader applicability of these findings[57,58]. Fourth, the CNSR-III cohort lacked information on socioeconomic status, educational level, and dietary habits, which are known to affect both brain aging and stroke recurrence[59–62]. Future studies should incorporate more comprehensive socioeconomic and lifestyle variables to better understand the mechanisms linking brain aging and cerebrovascular disease. Fifth, this study included only acute-phase stroke imaging data, lacking longitudinal follow-up imaging. Previous research have demonstrated that ischemic damage accelerates brain aging in stroke survivors[63]. Dynamic monitoring and assessment of brain age post-stroke could provide critical insights into the mechanisms underlying the interaction between brain aging and stroke, thereby offering valuable evidence to optimize intervention strategies.

In summary, this study demonstrates that BAG independently predicts both short-term and long-term stroke recurrence in patients with AICVD, showing superior predictive performance compared with chronological age. These findings support the utility of BAG as a radiomics-based metric for recurrence risk stratification and suggest a potential link between brain aging and stroke recurrence. Moreover, incorporating BAG into established prediction models improved discriminative accuracy, highlighting its potential to inform AI-guided, individualized strategies for secondary stroke prevention.

Methods

Study population

This study employed two publicly accessible datasets, along with a community cohort, to develop the brain age prediction model: OASIS, ADNI,

and PRECISE (Supplementary Table 1)[21–23]. The study protocol for PRECISE was approved by the ethics committees of both Beijing Tiantan Hospital (IRB approval number: KY2017-010-01) and Lishui Hospital (IRB approval number: 2016-42)[23]. Written informed consent was obtained from participants or their legal representatives. The brain age estimation networks were trained using data exclusively from healthy individuals, consisting of 5353 T2-FLAIR MRI scans. Notably, the ADNI and OASIS datasets included multiple follow-up scans for some participants, facilitating natural data augmentation.

In the clinical application phase, data from the CNSR-III study were utilized, including 10,890 patients with AIS or TIA who had high-quality T2-FLAIR and DWI imaging. The study design and imaging protocol of the CNSR-III has been previously described[24]. Briefly, the CNSR-III was a nationwide prospective registry conducted in China from August 2015 to March 2018, enrolling patients with AIS or TIA within 7 days of symptom onset at 201 hospitals across 22 provinces and 4 municipalities[24]. Ethical approval for the CNSR-III study was obtained from the ethics committee of Beijing Tiantan Hospital (IRB approval number: KY2015-001-01) and all participating centers. The participants or their legal representatives provided written informed consent.

Neuroimaging pre-processing

All T2-FLAIR images underwent a standardized pre-processing pipeline. Initial quality control (QC) was conducted on the raw Neuroimaging Informatics Technology Initiative (NIfTI) and Digital Imaging and Communications in Medicine (DICOM) data as part of the standardized imaging acquisition and quality assurance protocols established by the PRECISE and CNSR-III studies, as well as the included public datasets[23,24]. Only imaging data that met stringent QC criteria were advanced for further processing.

During the pre-processing stage, each T2-FLAIR image was first co-registered to a standardized T2-FLAIR template (GG-FLAIR-366, available at http://brainder.org)[64]. Image registration was performed using FLIRT (FMRIB's Linear Image Registration Tool) from the FSL (FMRIB Software Library) package, employing a rigid-body transformation with six degrees of freedom (three translational and three rotational parameters) to preserve anatomical fidelity while ensuring accurate spatial alignment. All images were resampled to an isotropic voxel resolution of 2 mm^3, yielding a consistent matrix size of $91 \times 109 \times 91$.

Following spatial registration, image quality was independently reviewed by two experienced radiologists. Exclusion criteria encompassed poor scan quality, severe head motion, substantial imaging artifacts, incomplete MRI acquisitions, and image distortions. Subsequently, brain extraction was performed using the SynthStrip algorithm, which provides robust delineation of brain tissue from non-brain structures[65]. After extraction, voxel intensities within the brain mask were normalized by mean-centering to zero and scaling to unit variance (standard deviation = 1). This intensity standardization was applied exclusively within the extracted brain regions to ensure consistent contrast normalization while preserving anatomical boundaries. All voxels outside the SynthStrip-derived brain mask (i.e., non-brain background) were assigned a fixed intensity value of −1, thereby ensuring anatomical consistency in the background representation and preventing the misclassification of brain tissue based on intensity values.

Development of the Mask-based Brain Age estimation Network

Figure 1a illustrated the training process of the MBA Net. The framework simultaneously input both masked and unmasked T2-FLAIR images, employing ScaledDense as the backbone network for feature extraction to predict the corresponding brain age values[26]. The ScaledDense network architecture is specifically designed to integrate multi-scale feature representations through densely connected pathways. Within each ScaledDense block, feature maps from preceding layers at varying spatial resolutions are resized using operations (max pooling) and subsequently concatenated. This multi-scale fusion mechanism enables the extraction of rich spatial information essential for accurate brain age estimation. Each layer in the ScaledDense block consists of two Asymmetric Convolution (AC) modules, batch normalization, an Exponential Linear Unit (ELU) activation function, a Squeeze-and-Excitation (SE) block, and max pooling. The AC module, tailored for three-dimensional (3D) MRI data, employs four distinct 3D convolutional kernels (e.g., $3 \times 3 \times 3$, $3 \times 1 \times 1$, $1 \times 3 \times 1$, $1 \times 1 \times 3$) to capture directional features across multiple orientations. The SE block recalibrates channel-wise feature responses by modeling inter-channel dependencies, thereby enhancing discriminative capability. ELU activations introduce non-linearity, enabling the network to learn complex feature mappings. Structurally, each ScaledDense block comprises five layers, with the initial layer containing eight channels. The channel width doubles with each subsequent layer (e.g., 8, 16, 32, 64, and 128 channels), allowing for progressive enhancement of representational capacity. Dense connectivity ensures that each layer receives direct inputs from all preceding layers and is connected to the final loss function, facilitating implicit deep supervision. This architectural design promotes efficient parameter utilization, mitigates overfitting, and improves gradient propagation, thereby enabling robust feature extraction from T2-FLAIR images.

Furthermore, the model used the difference between the predicted brain age and chronological age as loss functions. By incorporating consistency loss, the outputs of the brain age estimation model for masked and unmasked images remained consistent, thereby enhancing the accuracy and robustness of the predictions.

$$loss = loss_1 + loss_2 + \gamma loss_{consistency} \tag{1}$$

The MBA Net utilized the loss function defined in Eq. (1), which consisted of three components: the loss between the predicted brain age $\hat{y}$ from unmasked images and the chronological age y, as shown in Eq. (2); the loss between the predicted brain age $\hat{y}_{mask}$ from masked images and the chronological age y, as shown in Eq. (3); and the consistency loss between the predicted brain age $\hat{y}$ from unmasked images and the predicted brain age $\hat{y}_{mask}$ from masked images, as shown in Eq. (4). In these equations, $\hat{y}$ represented the predicted brain age from unmasked images, $\hat{y}_{mask}$ represented the predicted brain age from masked images, y represented the chronological brain age, and γ was the regularization parameter.

$$loss_1 = \mathcal{L}_r(y, \hat{y}) \tag{2}$$

$$loss_2 = \mathcal{L}_r(y, \hat{y}_{mask}) \tag{3}$$

$$loss_{consistency} = \mathcal{L}_r(\hat{y}, \hat{y}_{mask}) \tag{4}$$

where $\mathcal{L}_r$ denoted a loss function, which can be a mean squared error (MSE) loss or MAE loss.

To train the MBA Net using data from healthy individuals, this study employed randomly generated 3D rectangular masks to occlude portions of the input images. The use of rectangular (bounding box) masks for simulating lesions was guided by established regularization strategies in deep learning, such as the Cutout, wherein the geometric shape of the occluded region is generally considered less critical than its size and frequency[66]. This masking strategy offers a computationally efficient and standardized mechanism for simulating lesion-induced occlusions, thereby facilitating consistent implementation across varying anatomical and pathological configurations. The input data were processed according to the method outlined in Eq. (5) during the data loading phase, facilitating seamless integration with other data augmentation strategies.

$$\text{Mask Input Image} = x \odot M \tag{5}$$

where $x \in R^{H \times W \times D}$ represented the 3D MRI data. $M \in \{0, 1\}^{H \times W \times D}$ represented a binary mask, where a value of 1 indicated that the corresponding position in the original image would be preserved, while a value of 0 indicated that it would be masked. Additionally, the value of N was a

random integer that varied between 1 and 8, indicating that a different number of masks would be generated during each iteration. Given that the input consists of 3D MRI images, the generated masks were also 3D and exhibit a rectangular shape. Each mask could be uniquely determined by the tuple (x, y, z, l, w, h), where (x, y, z) represented the coordinates of the rectangle mask's center point, and (l, w, h) represented its respective length, width, and height.

In this study, we employed a random generation approach to define the tuple (x, y, z, l, w, h). Specifically, the center coordinates (x, y, z) were randomly selected near regions containing features, with the selection range constrained within a predefined spatial domain, as shown in Eq. (6).

$$(x, y, z) = (random(x_{\min}, x_{\max}), random(y_{\min}, y_{\max}), random(z_{\min}, z_{\max}) \quad (6)$$

Regarding the size of the cube mask, we established an upper limit d_{max} and a lower limit d_{min} to calculate the tuple (l, w, d) in Eq. (7).

$$(l, w, d) = (random(l_{\min}, l_{\max}), random(w_{\min}, w_{\max}), random(d_{\min}, d_{\max}) \quad (7)$$

We set the MSE loss as $\mathscr{L}_r$ and $\gamma = 5$ for training the MBA Net. The network was developed using the Adam optimization algorithm with a learning rate of 2e-4[67]. In addition, weight decay was applied with a coefficient of 1e-4. To enhance the reliability of gradient estimates, we aggregated the gradients across four mini-batches before each training step. The network was implemented using PyTorch (https://pytorch.org/). Data augmentation was conducted solely during the training phase, utilizing random flipping along the coronal axis and the addition of Gaussian noise. For the generation of brain masks, we defined the coordinate range for the mask center point to ($x_{min} = 20, x_{max} = 80$), ($y_{min} = 20, y_{max} = 100$) and ($z_{min} = 20, z_{max} = 80$), and the range for mask' size to $l_{min} = w_{min} = d_{min} = 5$ and $l_{max} = w_{max} = d_{max} = 30$.

Contextual brain age inferring for patients

As depicted in Fig. 1b, the process for inferring CBA in patients with AIS or TIA is as follows: (1) The DWI images of the subjects were first fed into a nnUNet model to generate a binary segmentation mask for acute ischemic lesions[25]; (2) A minimum bounding rectangle was subsequently derived from the segmentation map, producing a mask image that delineated a bounding box around the ischemic lesions; (3) The masked input image was then constructed by combining the generated mask with the T2-FLAIR image; (4) Finally, pre-trained MBA models were employed to analyze the masked input images, yielding the prediction of CBA. Furthermore, the predicted CBA underwent a bias correction, resulting in the final iteration of CBA.

The assessment of brain age often demonstrates a tendency to overestimate in younger individuals and underestimate in older individuals. As chronological age approaches the mean age, the estimated MAE tends to converge toward 0[68]. Statistical bias correction is commonly employed in the estimation of brain age or BAG[69]. In this study, we applied bias correction by fitting a linear regression model, as shown in Eq. (8).

$$\Omega \approx \alpha \cdot y + \beta \quad (8)$$

where y was the chronological age, α was the slope, β was the intercept, Ω was the offset for bias correction. The values of α and β were derived by fitting the linear regression model using the training dataset, then applied to the test dataset for bias correction. The offset was subtracted from the estimated brain age to obtain bias-corrected estimation for each test sample in Eq. (9):

$$\widetilde{y}_c \approx \widetilde{y} - (\alpha \cdot y + \beta) \quad (9)$$

where $\widetilde{y}_c$ was the bias-corrected brain age and $\widetilde{y}$ represented the estimated brain age.

In this study, BAG was calculated by subtracting chronological age from the CBA, as shown in Eq. (10).

$$\text{Brain Age Gap(BAG)} = \text{Contextual Brain Age(CBA)} - \text{chronological age} \quad (10)$$

Clinical information in patients with acute ischemic cerebrovascular disease

Trained research coordinators from the participating hospitals collected baseline data from medical records, including demographics, clinical characteristics, risk factors, medical history, primary diagnosis, and concomitant medication[24]. In addition, investigators conducted face-to-face interviews with patients upon admission to assess the pre-stroke mRS score, and evaluate the National Institutes of Health Stroke Scale (NIHSS) score. The Tiantan Neuroimaging Center of Excellence performed centralized etiological classification using the Trial of Org 10172 in Acute Stroke Treatment (TOAST) criteria, identifying five stroke subtypes: large-artery atherosclerosis, cardioembolism, small-vessel occlusion, other determined etiology, and undetermined etiology[41].

Clinical outcomes included recurrent stroke (ischemic or hemorrhagic stroke), composite vascular events (stroke, TIA, myocardial infarction, or vascular death), ischemic stroke, and hemorrhagic stroke. Patients were followed up through face-to-face interviews at 3 months and annual telephone interviews from 1 to 5 years[24]. The detailed definitions of clinical outcomes are presented in Supplementary Table 16.

Statistical analysis

Baseline characteristics were compared across groups. Continuous variables with skewed distributions were reported as medians with IQRs, and categorical variables as counts and percentages. The Wilcoxon rank-sum test was used to compare continuous variables between two groups, and the Kruskal–Wallis test was applied for comparisons among three groups. Categorical variables were compared using the χ^2 test.

Differences in BAG across baseline categorical variables were assessed using student's t-test. Variables demonstrating statistically significant differences in BAG were subsequently included in a multivariable linear regression model to identify independent determinants of BAG. The relationship between BAG and clinical outcomes was evaluated using multivariable Cox proportional hazards models. Additionally, Fine-Gray competing risk models were employed to account for death as a competing event. Adjusted models included BAG-related variables and clinical features of the index event, such as admission diagnosis, NIHSS score, TOAST classification, and infarct volume.

Sensitivity analysis was conducted by categorizing BAG as either a binary or three-level variable. When BAG was analyzed as a categorical variable in relation to clinical outcomes, multivariable models were adjusted for baseline characteristics that significantly differed between groups (Supplementary Tables 5 and 7), as well as clinical features of the index event, including admission diagnosis, NIHSS score, TOAST classification. Given the exploratory nature of this study investigating the association between BAG and stroke recurrence, we did not apply multiple testing corrections to avoid obscuring potentially significant clinical findings. Time to outcome events were graphically presented using Kaplan–Meier curves and compared by the log-rank test.

The predictive performance of BAG for clinical outcomes was evaluated from three perspectives. First, its prognostic utility was compared with that of chronological age. Model discrimination was assessed with Harrell's C statistic, and calibration was evaluated using the Brier score. Second, the incremental value of BAG was examined by incorporating it into established clinical prediction models, with its contribution quantified using NRI and IDI. Third, to further assess its contribution to risk prediction, BAG was integrated into multivariable Cox proportional hazards models that included age, sex, BMI, history of ischemic stroke, TIA, coronary heart disease, hypertension, diabetes mellitus, hypercholesterolemia, smoking status,

index event, NIHSS score on admission, pre-stroke mRS score, and TOAST classification.

Two-sided p values < 0.05 indicated statistical significance. Calculations of NRI and IDI, as well as the generation of violin plots, were performed using R software (V4.5.0). All other statistical analyses were conducted using SAS software (V 9.4).

Data availability

The data from the ADNI database (adni.loni.usc.edu) and the OASIS database (https://www.oasis-brains.org/) are publicly accessible. The anonymized data from the PRECISE study and the CNSR-III study are available to fellow researchers on request for replicating procedures or reproducing the results by contacting the corresponding author and their institutions.

Code availability

Researchers can access the code at GitHub: [https://github.com/liuziyang1106/MBA_Net_for_ContexualBrainAge].

Received: 23 February 2025; Accepted: 7 November 2025;
Published online: 08 December 2025

References

1. Hobeanu, C. et al. Risk of subsequent disabling or fatal stroke in patients with transient ischaemic attack or minor ischaemic stroke: an international, prospective cohort study. *Lancet Neurol.* **21**, 889–898 (2022).
2. Wang, Y. et al. Ticagrelor versus clopidogrel in *CYP2C19* loss-of-function carriers with stroke or TIA. *N. Engl. J. Med.* **385**, 2520–2530 (2021).
3. Jiang, L. et al. Radiomics analysis of diffusion-weighted imaging and long-term unfavorable outcomes risk for acute. *Stroke* **54**, 488–498 (2023).
4. Jones, D. T., Lee, J. & Topol, E. J. Digitising brain age. *Lancet* **400**, 988 (2022).
5. Chung, Y. et al. Use of machine learning to determine deviance in neuroanatomical maturity associated with future psychosis in youths at clinically high risk. *JAMA Psychiatry* **75**, 960–968 (2018).
6. Habes, M. et al. The Brain Chart of Aging: machine-learning analytics reveals links between brain aging, white matter disease, amyloid burden, and cognition in the iSTAGING consortium of 10,216 harmonized MR scans. *Alzheimers Dement* **17**, 89–102 (2021).
7. Gonneaud, J. et al. Accelerated functional brain aging in pre-clinical familial Alzheimer's disease. *Nat. Commun.* **12**, 5346 (2021).
8. Liew, S. L. et al. Association of brain age, lesion volume, and functional outcome in patients with stroke. *Neurology* **100**, e2103–e2113 (2023).
9. Cole, J. H., Marioni, R. E., Harris, S. E. & Deary, I. J. Brain age and other bodily 'ages': implications for neuropsychiatry. *Mol. Psychiatry* **24**, 266–281 (2019).
10. Dintica, C. S. et al. Elevated blood pressure is associated with advanced brain aging in mid-life: a 30-year follow-up of The CARDIA Study. *Alzheimers Dement* **19**, 924−932 (2023).
11. Rauseo, E. et al. Ischemic heart disease and vascular risk factors are associated with accelerated brain aging. *JACC Cardiovasc. Imaging* **16**, 905–915 (2023).
12. Mo, C. et al. Evaluating the causal effect of tobacco smoking on white matter brain aging: a two-sample Mendelian randomization analysis in UK Biobank. *Addiction* **118**, 739–749 (2023).
13. Wagen, A. Z. et al. Life course, genetic, and neuropathological associations with brain age in the 1946 British Birth Cohort: a population-based study. *Lancet Healthy Longev.* **3**, e607–e616 (2022).
14. Pan, Y. et al. Time course for benefit and risk with ticagrelor and aspirin in individuals with acute ischemic stroke or transient ischemic attack who carry *CYP2C19* loss-of-function alleles: a secondary analysis of the CHANCE-2 randomized clinical trial. *JAMA Neurol.* **79**, 739–745 (2022).
15. Powers, W. J. et al. Guidelines for the early management of patients with acute ischemic stroke: 2019 update to the 2018 guidelines for the early management of acute ischemic stroke: a guideline for healthcare professionals from the American Heart Association/American Stroke Association. *Stroke* **50**, e344–e418 (2019).
16. Dawson, J. et al. European Stroke Organisation expedited recommendation for the use of short-term dual antiplatelet therapy early after minor stroke and high-risk TIA. *Eur. Stroke J.* **6**, Clxxxvii–cxci (2021).
17. Liu, L. et al. Chinese Stroke Association guidelines for clinical management of ischaemic cerebrovascular diseases: executive summary and 2023 update. *Stroke Vasc. Neurol.* **8**, e3 (2023).
18. Bretzner, M. et al. Radiomics-derived brain age predicts functional outcome after acute ischemic stroke. *Neurology* **100**, e822−e833 (2023).
19. Busby, N. et al. Advanced brain age and chronic poststroke aphasia severity. *Neurology* **100**, e1166–e1176 (2023).
20. Thomalla, G. et al. Intravenous alteplase for stroke with unknown time of onset guided by advanced imaging: systematic review and meta-analysis of individual patient data. *Lancet* **396**, 1574–1584 (2020).
21. Pamela, J. L. et al. OASIS-3: longitudinal neuroimaging, clinical, and cognitive dataset for normal aging and Alzheimer disease. Preprint at https://doi.org/10.1101/2019.12.13.19014902 (2019).
22. Weiner, M. W. et al. The Alzheimer's Disease Neuroimaging Initiative 3: continued innovation for clinical trial improvement. *Alzheimers Dement.* **13**, 561–571 (2017).
23. Pan, Y. et al. PolyvasculaR Evaluation for Cognitive Impairment and vaScular Events (PRECISE)-a population-based prospective cohort study: rationale, design and baseline participant characteristics. *Stroke Vasc. Neurol.* **6**, 145–151 (2021).
24. Wang, Y. et al. The Third China National Stroke Registry (CNSR-III) for patients with acute ischaemic stroke or transient ischaemic attack: design, rationale and baseline patient characteristics. *Stroke Vasc. Neurol.* **4**, 158–164 (2019).
25. Jing, J. et al. A deep learning system to predict recurrence and disability outcomes in patients with transient ischemic attack or ischemic stroke. *Adv. Intell. Syst.* **5**, 2200240 (2023).
26. Cheng, J. et al. Brain age estimation from MRI using cascade networks with ranking loss. *IEEE Trans. Med Imaging* **40**, 3400–3412 (2021).
27. Kernan, W. N., Horwitz, R. I., Brass, L. M., Viscoli, C. M. & Taylor, K. J. A prognostic system for transient ischemia or minor stroke. *Ann. Intern. Med.* **114**, 552–557 (1991).
28. Kernan, W. N. et al. The stroke prognosis instrument II (SPI-II): a clinical prediction instrument for patients with transient ischemia and nondisabling ischemic stroke. *Stroke* **31**, 456–462 (2000).
29. Weimar, C. et al. The Essen stroke risk score predicts recurrent cardiovascular events: a validation within the REduction of Atherothrombosis for Continued Health (REACH) registry. *Stroke* **40**, 350–354 (2009).
30. Ay, H. et al. A score to predict early risk of recurrence after ischemic stroke. *Neurology* **74**, 128–135 (2010).
31. Merwick, A. et al. Addition of brain and carotid imaging to the ABCD^2 score to identify patients at early risk of stroke after transient ischaemic attack: a multicentre observational study. *Lancet Neurol.* **9**, 1060–1069 (2010).
32. Duering, M. et al. Neuroimaging standards for research into small vessel disease-advances since 2013. *Lancet Neurol.* **22**, 602−618 (2023).
33. Nam, K. W. et al. FLAIR vascular hyperintensities predict early ischemic recurrence in TIA. *Neurology* **90**, e738–e744 (2018).
34. Mossa-Basha, M. & Zhu, C. White matter hyperintensities and their relationship to outcomes after stroke intervention. *Radiology* **304**, 153–154 (2022).

35. Thomalla, G. et al. MRI-guided thrombolysis for stroke with unknown time of onset. *N. Engl. J. Med.* **379**, 611–622 (2018).
36. Du, J. et al. White matter brain age as a biomarker of cerebrovascular burden in the ageing brain. *Eur. Arch. Psychiatry Clin. Neurosci.* https://doi.org/10.1007/s00406-024-01758-3 (2024).
37. Huang, C. C. et al. Brain white matter hyperintensities-predicted age reflects neurovascular health in middle-to-old aged subjects. *Age Ageing* **51**, afac106 (2022).
38. Scheldeman, L. et al. Early penumbral FLAIR changes predict tissue fate in patients with large vessel occlusions. *Int. J. Stroke* **20**, 310–318 (2025).
39. Albers, G. W. Diffusion-weighted MRI for evaluation of acute stroke. *Neurology* **51**, S47–S49 (1998).
40. Wang, A. et al. Bleeding risk of dual antiplatelet therapy after minor stroke or transient ischemic attack. *Ann. Neurol.* **91**, 380–388 (2022).
41. Adams, H. P. Jr et al. Classification of subtype of acute ischemic stroke. Definitions for use in a multicenter clinical trial. TOAST. Trial of Org 10172 in Acute Stroke Treatment. *Stroke* **24**, 35–41 (1993).
42. Lioutas, V. A. et al. Incidence of transient ischemic attack and association with long-term risk of stroke. *Jama* **325**, 373–381 (2021).
43. de Lange, A. G. et al. Multimodal brain-age prediction and cardiovascular risk: the Whitehall II MRI sub-study. *Neuroimage* **222**, 117292 (2020).
44. Oh, H. S. et al. Organ aging signatures in the plasma proteome track health and disease. *Nature* **624**, 164–172 (2023).
45. Korbmacher, M. et al. Brain asymmetries from mid- to late life and hemispheric brain age. *Nat. Commun.* **15**, 956 (2024).
46. Lee, J. et al. Deep learning-based brain age prediction in normal aging and dementia. *Nat. Aging* **2**, 412–424 (2022).
47. Jonsson, B. A. et al. Brain age prediction using deep learning uncovers associated sequence variants. *Nat. Commun.* **10**, 5409 (2019).
48. Chu, L. X. et al. Spatiotemporal multi-omics: exploring molecular landscapes in aging and regenerative medicine. *Mil. Med. Res.* **11**, 31 (2024).
49. Lu, A. T. et al. Genetic architecture of epigenetic and neuronal ageing rates in human brain regions. *Nat. Commun.* **8**, 15353 (2017).
50. Zhang, X. et al. Telomere length and stroke recurrence after ischemic stroke and TIA. *Int. J. Stroke* **18**, 208–214 (2023).
51. Jha, M. K., Chin Fatt, C., Minhajuddin, A., Mayes, T. L. & Trivedi, M. H. Accelerated brain aging in adults with major depressive disorder predicts poorer outcome with sertraline: findings from the EMBARC study. *Biol. Psychiatry Cogn. Neurosci. Neuroimaging* **8**, 462–470 (2023).
52. Van Gestel, H. et al. Brain age in bipolar disorders: effects of lithium treatment. *Aust. N. Z. J. Psychiatry* **53**, 1179–1188 (2019).
53. He, S. et al. Human-to-monkey transfer learning identifies the frontal white matter as a key determinant for predicting monkey brain age. *Front Aging Neurosci.* **15**, 1249415 (2023).
54. Brusini, I. et al. MRI-derived brain age as a biomarker of ageing in rats: validation using a healthy lifestyle intervention. *Neurobiol. Aging* **109**, 204–215 (2022).
55. Haugg, F. et al. Imaging biomarkers of ageing: a review of artificial intelligence-based approaches for age estimation. *Lancet Healthy Longev.* **6**, 100728 (2025).
56. Rodríguez Mallma, M. J. et al. Explainable machine learning models for brain diseases: insights from a systematic review. *Neurol. Int.* **16**, 1285–1307 (2024).
57. Dichgans, M., Pulit, S. L. & Rosand, J. Stroke genetics: discovery, biology, and clinical applications. *Lancet Neurol.* **18**, 587–599 (2019).
58. Harshfield, E. L., Georgakis, M. K., Malik, R., Dichgans, M. & Markus, H. S. Modifiable lifestyle factors and risk of stroke: a Mendelian randomization analysis. *Stroke* **52**, 931–936 (2021).
59. Busby, N. et al. Lower socioeconomic status is associated with premature brain aging. *Neurobiol. Aging* **130**, 135–140 (2023).
60. Clocchiatti-Tuozzo, S. et al. Life's essential 8 and poor brain health outcomes in middle-aged adults. *Neurology* **103**, e209990 (2024).
61. Stulberg, E. L. et al. Correlations of socioeconomic and clinical determinants with United States county-level stroke prevalence. *Ann. Neurol.* **96**, 739–744 (2024).
62. Collaborators, G. S. R. F. Global, regional, and national burden of stroke and its risk factors, 1990-2021: a systematic analysis for the Global Burden of Disease Study 2021. *Lancet Neurol.* **23**, 973–1003 (2024).
63. Egorova, N., Liem, F., Hachinski, V. & Brodtmann, A. Predicted brain age after stroke. *Front Aging Neurosci.* **11**, 348 (2019).
64. Kochunov, P. et al. Retrospective motion correction protocol for high-resolution anatomical MRI. *Hum. Brain Mapp.* **27**, 957–962 (2006).
65. Hoopes, A., Mora, J. S., Dalca, A. V., Fischl, B. & Hoffmann, M. SynthStrip: skull-stripping for any brain image. *Neuroimage* **260**, 119474 (2022).
66. DeVries, T. & Taylor, G. W. Improved regularization of convolutional neural networks with cutout. Preprint at https://arxiv.org/abs/1708.04552 (2017).
67. Kingma, D. P. & Ba, J. Adam: a method for stochastic optimization. Preprint at https://arxiv.org/abs/1412.6980 (2014).
68. Smith, S. M., Vidaurre, D., Alfaro-Almagro, F., Nichols, T. E. & Miller, K. L. Estimation of brain age delta from brain imaging. *Neuroimage* **200**, 528–539 (2019).
69. Liang, H., Zhang, F. & Niu, X. Investigating systematic bias in brain age estimation with application to post-traumatic stress disorders. *Hum. Brain Mapp.* **40**, 3143–3152 (2019).

Acknowledgements

This work was supported by grants from the National Key Research and Development Program of China (2022YFC2504900), grants from the Beijing Natural Science Foundation (Z200016), grants from the National Natural Science Foundation of China (82372040, U20A20358), and grants from the Chinese Academy of Medical Sciences Innovation Fund for Medical Sciences (2019-I2M-5-029).

Author contributions

Y.W.[1], T.L., Z.L.[2], H.Z., and Z.L.[3] conceptualized and designed the study. H.Z., Z.L.[3], J.J., L.D., Y.P., Y.J.[4], X.M., and X.X. were responsible for collecting clinical and imaging data. Z.L.[3] led the construction and validation of the deep learning model, with technical support from T.L., H.L.[5], J.Z., J.C., W.Z., Z.Z., and Y.F. in algorithm design and implementation. H.Z., H.G., and Y.J.[6] conducted statistical analyses and created the data visualizations. Y.W.[7], X.Z., H.L.[8], and J.Z. provided guidance on the statistical methodologies. H.Z. and Z.L.[3] drafted the initial manuscript, which was revised with contributions from Y.W.[1] (clinical aspects), T.L. (deep learning) and Z.L.[2] (statistics). All authors reviewed and approved the final manuscript. [1]Yongjun Wang, [2]Zixiao Li, [3]Ziyang Liu, [4]Yong Jiang, [5]Hao Liu, [6]Yingyu Jiang, [7]Yilong Wang, [8]Hao Li.

Competing interests

The authors declare no competing interests.

Additional information

Supplementary information The online version contains supplementary material available at https://doi.org/10.1038/s41746-025-02161-5.

Correspondence and requests for materials should be addressed to Zixiao Li, Tao Liu or Yongjun Wang.